EUROPEAN ORGANIZATION FOR NUCLEAR RESEARCH

L3 Note 2749
June 25, 2002

Search for Neutral Higgs Bosons of the Minimal Supersymmetric Standard Model in e^+e^- Interactions at $\sqrt{s}$ up to 209 GeV

The L3 Collaboration

Abstract

A search for the lightest neutral CP-even and neutral CP-odd Higgs bosons of the Minimal Supersymmetric Standard Model is performed using 216.6 pb^{-1} of data collected with the L3 detector at LEP at centre-of-mass energies between 203 and 209 GeV. No indication of a signal is found. Including our results from lower centre-of-mass energies, lower limits on the Higgs bosons masses are set as a function of $\tan\beta$ for several scenarios. For all the scenarios considered, the mass limits for $\tan\beta$ greater than 0.7 are $m_{\mathrm{h}} > 84.5$ GeV and $m_{\mathrm{A}} > 86.3$ GeV at 95% confidence level.

ALL RESULTS QUOTED IN THIS NOTE ARE PRELIMINARY

Submitted to the 31^{st} *International Conference on High Energy Physics*
Amsterdam, Netherlands, 24-31 July 2002.

1 Introduction

In the Minimal Supersymmetric Standard Model (MSSM) [1] two doublets of complex scalar fields are required to generate the masses of gauge bosons and fermions. The neutral Higgs sector of the MSSM comprises three physical states: two CP-even Higgs bosons, the lighter of which is denoted as h and the heavier as H, and a neutral CP-odd boson, A.

The two most important production mechanisms of the light neutral Higgs boson in e^+e^- collisions are:

$$e^+e^- \to hZ, \tag{1}$$

$$e^+e^- \to hA, \tag{2}$$

with tree level cross sections that are related to the Standard Model Higgs-strahlung cross section, σ_{HZ}^{SM}, as follows [2]:

$$\sigma_{hZ} = \sin^2(\beta-\alpha)\sigma_{HZ}^{SM}, \tag{3}$$

$$\sigma_{hA} = \cos^2(\beta-\alpha)\tilde{\lambda}\sigma_{HZ}^{SM}, \tag{4}$$

where $\tan\beta$ is the ratio of vacuum expectation values of the two Higgs doublets, α is the mixing angle in the CP-even Higgs boson sector and $\tilde{\lambda}$ is the p-wave suppression factor depending on the Higgs boson masses m_h and m_A and the centre-of-mass energy $\sqrt{s}$. For some choices of the MSSM parameters the H boson can be produced in the centre-of-mass energy range of this study via the Higgs-strahlung process

$$e^+e^- \to HZ, \tag{5}$$

with a cross section suppressed by the factor $\cos^2(\beta-\alpha)$ relative to σ_{HZ}^{SM}.

For most of the MSSM parameter space considered, the neutral Higgs bosons are predicted to decay dominantly to $b\bar{b}$ and $\tau^+\tau^-$. However, in certain parameter regions, other decays like $h \to AA$ and $A \to c\bar{c}$ become important.

The search for the neutral Higgs bosons is performed in the framework of the constrained MSSM with seven free parameters. These are the universal sfermion mass parameter, M_{SUSY}, the common Higgs-squark trilinear coupling, $\mathcal{A}$, the supersymmetric Higgs mass parameter, μ, the SU(2) gaugino mass parameter, M_2, the gluino mass parameter, M_3, m_A and $\tan\beta$. The mass of the top quark is taken to be 174.3 GeV [3].

Previous searches for the neutral Higgs bosons were reported by L3 [4] and other experiments [5]. In this paper, we present the results of the search for the h and A bosons using data collected with the L3 detector [6] in the year 2000. In comparison to previous analyses [4] the performance in the four-jet channel is improved by using a new likelihood based analysis. In addition the six-jet final state resulting from the $hZ \to AAq\bar{q}$ topology is investigated.

2 Benchmark Scenarios

Due to the large number of parameters remaining in the constrained MSSM we focus on three specific parameter settings as suggested in Ref. [7]. These benchmark settings are denoted as the "m_h-max", "no mixing" and "large-μ" scenarios, with corresponding MSSM parameter values detailed in Table 1. The first two scenarios take into account radiative corrections to m_h computed within a two-loop diagrammatic approach [8, 9] and differ only by the value of $X_t \equiv \mathcal{A} - \mu\cot\beta$ which governs the mixing in the scalar top sector. The "m_h-max" scenario is designed to extend the search to the maximal theoretical bound on m_h for any value of $\tan\beta$

and leads to rather conservative constraints on tanβ. The "no mixing" scenario corresponds to vanishing mixing in the scalar top sector and is more favorable to LEP searches. After fixing the parameters M_{SUSY}, M_2, μ, X_t and M_3, a scan over the remaining parameters tanβ and m_A is performed in the range $0.4 \leq \tan\beta \leq 30$ and 10 GeV $\leq m_A \leq 1$ TeV. The widths of h and A bosons are assumed to be smaller than the experimental mass resolutions. As this holds in these two scenarios only for tan$\beta \leq 30$, higher values of tanβ are not considered.

In the "large-μ" scenario the upper theoretical bound on m_h is slightly less than 108 GeV, allowing the entire (tanβ,m_h) plane to be kinematically covered using LEP results. For some choices of tanβ and m_A the Higgs boson pair production (2) is kinematically inaccessible and the Higgs-strahlung process (1) is strongly suppressed due to small values of $\sin^2(\beta-\alpha)$. However for these regions the H boson mass is less than 109 GeV allowing relatively high cross-section production by the Higgs-strahlung process. But within this scenario the coupling of h or H to $b\bar{b}$ can be considerably suppressed due to loop corrections [10,11] making searches difficult in these regions. The scan is performed over m_A from 10 GeV to 400 GeV and over tanβ between 0.7 and 50. Within this scenario the assumption that the widths of the Higgs bosons are small compared to experimental mass resolutions is valid for tanβ up to 50. For the interpretation of the data within this "large-μ" scenario, the improved one-loop renormalisation group calculations [11–13] are used.

3 Data and Monte Carlo Samples

The data recorded during the year 2000 at centre-of-mass energies between 203 and 209 GeV, are grouped into three data sets with effective centre-of-mass energies of 204.3, 206.1 and 208.0 GeV corresponding to luminosities of 26.0, 181.9 and 8.7 pb^{-1}. The results obtained from this data are combined with the results from luminosities of 233.2 pb^{-1} at 192 GeV $< \sqrt{s} <$ 202 GeV and 176.4 pb^{-1} at $\sqrt{s} = 189$ GeV.

The cross sections of processes (1), (2) and (5) and the decay branching fractions of h, H and A are calculated using the HZHA generator [14]. For efficiency studies, Monte Carlo samples of 2000 Higgs events are generated for each mass hypothesis using PYTHIA [15] and HZHA. For the hA samples, m_h and m_A range from 50 to 105 GeV in steps of 5 GeV. For the hZ samples, m_h is chosen in steps of 5 GeV from 60 to 100 GeV and in steps of 1 GeV from 100 to 120 GeV. For background studies, the following Monte Carlo programs are used: KK2f [16] ($e^+e^- \to q\bar{q}(\gamma)$), PYTHIA ($e^+e^- \to ZZ$ and $e^+e^- \to Ze^+e^-$), KORALW [17] ($e^+e^- \to W^+W^-$) and KORALZ [18] ($e^+e^- \to \tau^+\tau^-$). Hadron production in two-photon interactions is simulated with PYTHIA and PHOJET [19]. EXCALIBUR [20] is used for other four fermion final states. The number of simulated events for the most important background channels is more than 100 times the number of expected events.

The L3 detector response is simulated using the GEANT program [21], which models the effects of energy loss, multiple scattering and showering in the detector. The GHEISHA program [22] is used to simulate hadronic interactions in the detector. Time dependent detector inefficiencies, monitored during data taking, are also taken into account.

4 Analysis Procedures

For hA production, the decay modes considered are: $hA \to b\bar{b}b\bar{b}$, $hA \to b\bar{b}\tau^+\tau^-$ and $hA \to \tau^+\tau^-b\bar{b}$. For hZ or HZ production, the event topologies considered are: $q\bar{q}q'\bar{q}'$, $q\bar{q}\nu\bar{\nu}$, $q\bar{q}\ell^+\ell^-(\ell = e, \mu, \tau)$

and $\tau^+\tau^-\mathrm{q\bar{q}}$. To cover the MSSM parameter regions where the decay $\mathrm{h} \to \mathrm{AA}$ becomes important, the $\mathrm{hZ} \to \mathrm{AAq\bar{q}} \to \mathrm{q\bar{q}q'\bar{q}'q''\bar{q}''}$ channel is studied as well. Searches in channels with decays of the h boson into quarks are optimised for the dominant $\mathrm{h} \to \mathrm{b\bar{b}}$ decay channel. The analyses of the $\mathrm{q\bar{q}}\nu\bar{\nu}$ and $\mathrm{q\bar{q}}\ell^+\ell^-(\ell = \mathrm{e}, \mu)$ final states are the same as those used in the Standard Model Higgs search [23].

4.1 The $\mathrm{hZ} \to \mathrm{b\bar{b}q\bar{q}}$ and $\mathrm{hA} \to \mathrm{b\bar{b}b\bar{b}}$ Analyses

The signature of the $\mathrm{hZ} \to \mathrm{b\bar{b}q\bar{q}}$ final state is four high-multiplicity hadronic jets and the presence of b hadrons, in particular in the jets expected to stem from the Higgs boson. The invariant mass of the jets presumably originating from the Z boson must be compatible within mass resolution with m_{Z}. The $\mathrm{hA} \to \mathrm{b\bar{b}b\bar{b}}$ search topology is characterised by four high multiplicity hadronic jets originating from b-quarks. The main backgrounds arise from $\mathrm{q\bar{q}}(\gamma)$ final states and hadronic decays of W- and Z-pairs.

Initially, a common preselection for both the $\mathrm{hZ} \to \mathrm{b\bar{b}q\bar{q}}$ and $\mathrm{hA} \to \mathrm{b\bar{b}b\bar{b}}$ channels is applied, followed by a kinematic classification of events into hZ or hA analysis branches. Selection criteria optimised for each branch are used and a final discriminant specific to each branch is constructed.

The preselection criteria used are described in Ref. [23]. Events passing the preselection are forced into a four-jet topology using the Durham algorithm [24] and a kinematic fit imposing energy and momentum conservation (4C fit) is performed. Each event is tested for its compatibility with the hZ and hA production hypotheses exploiting dijet invariant masses. There are three possibilities for pairing jets in a four-jet event. For each pairing, χ^2 values are calculated for the hypotheses of hZ and hA production:

$$\chi^2_{\mathrm{hZ}} = \frac{(\Sigma_{\mathrm{i}} - m_{\mathrm{h}} - m_{\mathrm{Z}})^2}{\sigma^2_{\Sigma}} + \frac{(\Delta_{\mathrm{i}} - |m_{\mathrm{h}} - m_{\mathrm{Z}}|)^2}{\sigma^2_{\Delta}}, \tag{6}$$

$$\chi^2_{\mathrm{hA}} = \frac{(\Sigma_{\mathrm{i}} - m_{\mathrm{h}} - m_{\mathrm{A}})^2}{\sigma^2_{\Sigma}} + \frac{(\Delta_{\mathrm{i}} - |m_{\mathrm{h}} - m_{\mathrm{A}}|)^2}{\sigma^2_{\Delta}}. \tag{7}$$

In these expressions Σ_{i} and Δ_{i} are dijet mass sum and dijet mass difference of the i-th pairing, and σ_{Σ} and σ_{Δ} are the dijet mass sum and dijet mass difference resolution functions. They are found to be almost independent of the dijet masses for production well above threshold and are estimated from Monte Carlo to be $\sigma_{\Sigma} = 4\,\mathrm{GeV}$ and $\sigma_{\Delta}/\sigma_{\Sigma} = 4.6$. Close to the kinematic threshold they strongly depend on the dijet mass sum and are parametrised as a function of Σ. For each hypothesis, the jet pairing with the smallest χ^2 is chosen and the probability $\mathrm{P}(\chi^2)$ is calculated.

Events are assigned either to the hZ or hA analysis branch by means of a binned likelihood [23], $\mathrm{L}^{\mathrm{c}}_{\mathrm{hZ}} \equiv 1 - \mathrm{L}^{\mathrm{c}}_{\mathrm{hA}}$, constructed from the following variables: the χ^2 probabilities, $\mathrm{P}(\chi^2_{\mathrm{hA}})$ and $\mathrm{P}(\chi^2_{\mathrm{hA}})$, the Higgs boson production angle, $|\cos\Theta|$, the maximum triple jet boost, γ_{triple}, the number of charged tracks, $\mathrm{N}_{\mathrm{trk}}$, and the global event b-tag, $\mathrm{B}_{\mathrm{tag}}$ [23]. Events are assigned to the hZ branch if $\mathrm{L}^{\mathrm{c}}_{\mathrm{hZ}} > 0.5$, or to the hA branch otherwise.

The selection in both branches proceeds in the same way. Events are rejected if $\mathrm{P}(\chi^2) < 1\%$. The global event b-tag is required to be greater than 1.0 and 0.36 for events classified as hA and hZ, respectively. The selection likelihood is then constructed to separate the signal from the ZZ, WW and $\mathrm{q\bar{q}}(\gamma)$ final states, using $\mathrm{N}_{\mathrm{trk}}$, $\mathrm{B}_{\mathrm{tag}}$, γ_{triple}, $|\cos\Theta|$ and $\log\mathrm{Y}_{34}$, where Y_{34} is the jet resolution parameter for which the event topology changes from four-jet to three-jet.

The final discriminant is constructed for events passing an optimised selection likelihood cut. The optimisation is based on analysis performance at ($m_{\rm A}$,$m_{\rm h}$) values close to the expected sensitivity of the L3 combined search. The final discriminants are built from individual b-tag variables of the four jets and P(χ^2). In the hZ branch an event category variable is also used, this variable is constructed from rankings of b-tag variables of the two jets assigned to the Higgs boson, as described in Ref. [23]. The final discriminant in the hA branch also includes the corresponding selection likelihood.

Table 2 reports the number of data, expected background and expected signal events selected at different stages of the analysis for two representative Higgs boson mass hypotheses in the "$m_{\rm h}$-max" scenario, ($m_{\rm A}$,$m_{\rm h}$) = (90,90) GeV at tanβ = 25 and ($m_{\rm A}$,$m_{\rm h}$) = (165,110) GeV at tanβ = 3. For these hypotheses the distribution of the final discriminant in terms of a signal-to-background ratio is presented in Figure 1 for data, the expected background and the expected signal. The data are compatible with the background expectation.

4.2 The $\rm hZ \to b\bar{b}\tau^+\tau^-, \tau^+\tau^-q\bar{q}$ and $\rm hA \to b\bar{b}\tau^+\tau^-$ Analyses

The signatures of $\rm hZ \to b\bar{b}\tau^+\tau^-, \tau^+\tau^-q\bar{q}$ and $\rm hA \to b\bar{b}\tau^+\tau^-$ [1)] final states are a pair of taus accompanied by two hadronic jets. For each of the channels hA and hZ an analysis is optimised based either on the tau identification or on the event topology by requiring four jets with two of them being narrow and of low multiplicity. The main background comes from W-pair decays containing taus. The analysis is similar to the one used in previous searches [4]. The selection is optimised for lower Higgs boson masses by applying looser cuts on the opening angles of the jets and tau pairs compared to the Standard Model Higgs search [23]. The invariant mass of the tau pair, $m_{\tau^+\tau^-}$, and of the hadronic jets, $m_{\rm q\bar{q}}$, must be between 25 GeV and 125 GeV. The ratio between the total energy deposited in the detector, $\rm E_{vis}$, and $\sqrt{s}$ must be less than 0.9 and the polar angle of the missing momentum, $\Theta_{\rm miss}$, must be $|\cos\Theta_{\rm miss}| < 0.9$.

Four possible final states are considered: $\rm hZ \to b\bar{b}\tau^+\tau^-$, $\rm hZ \to \tau^+\tau^-q\bar{q}$, $\rm hA \to b\bar{b}\tau^+\tau^-$ and $\rm hA \to \tau^+\tau^-b\bar{b}$. Each event is uniquely assigned to one channel using mass and b-tag information, and final discriminants specific to each channel are constructed. For the $\rm hZ \to b\bar{b}\tau^+\tau^-$, $\rm hA \to b\bar{b}\tau^+\tau^-$ and $\rm hA \to \tau^+\tau^-b\bar{b}$ final states, the final discriminant is constructed from $m_{\rm q\bar{q}}$, $m_{\tau^+\tau^-}$ and the b-tag variables of the two hadronic jets. For the $\rm hZ \to \tau^+\tau^-q\bar{q}$ final state, $m_{\tau^+\tau^-}$ is used as the final discriminant.

Table 3 reports the number of data, expected background and expected signal events for the same Higgs boson masses chosen in the previous section. For these hypotheses the distribution of the final discriminant in terms of a signal-to-background ratio is shown in Figure 2 for the data, the expected background and the expected signal. Good agreement between the data and the expected background is found.

4.3 The $\rm hZ \to AAq\bar{q}$ Channel

To improve search sensitivity in the region of low tanβ and low $m_{\rm A}$ where the $\rm h \to AA$ decay becomes dominant and $\rm A \to c\bar{c}$ replaces $\rm A \to b\bar{b}$, a dedicated analysis is developed and performed on the data collected at $\sqrt{\rm s}$ = 189 - 209 GeV. This analysis aims to select $\rm hZ \to AAq\bar{q} \to q\bar{q}q'\bar{q}'q''\bar{q}''$ final states and is devised from the analysis used in the four-jet channel. At the first stage, the same preselection as in the four-jet channel is applied with an additional cut on the event thrust, T < 0.9. In the next step, a signal likelihood $\rm L_{AAqq}$ is built

[1)] Both of the decay modes ($\rm h \to b\bar{b}$, $\rm A \to \tau^+\tau^-$) and ($\rm h \to \tau^+\tau^-$, $\rm A \to b\bar{b}$) are considered.

to distinguish the $hZ \to AAq\bar{q}$ signal from the ZZ, WW and $q\bar{q}(\gamma)$ backgrounds. The L_{AAqq} is constructed from the variables: N_{trk}, γ_{triple}, $\log Y_{34}$, the event sphericity, the absolute value of the cosine of the polar production angle assuming the production of a pair of gauge bosons, $|\cos\Theta_{2B}|$ [23], and $\log Y_{56}$, where Y_{56} is the jet resolution parameter for which an event topology changes from six-jet to five-jet. Among these variables N_{trk} and $\log Y_{56}$ have the most discriminating power between the $hZ \to AAq\bar{q}$ signal and four-fermion and two-fermion backgrounds. The likelihood L_{AAqq} is used as the final discriminant. No evidence for the $hZ \to AAq\bar{q}$ signal is found in data. As an example Figure 3 shows the distributions of $\log Y_{56}$ and $L_{AAq\bar{q}}$ for data collected in the year 2000, the expected background and the signal corresponding to the Higgs boson mass hypothesis (m_A,m_h) = (30,70) GeV.

5 Results

The final discriminant distributions obtained in each search channel at each centre-of-mass energy are combined and used to estimate the consistency of the observation with "background-only" and "signal+background" hypotheses at each point of the (tanβ,m_A) scan in the three benchmark scenarios. The statistical procedure adopted for the interpretation of the data and the definitions of the confidence levels $(1 - CL_b)$, CL_{s+b} and CL_s are described in Ref. [25]. The confidence levels $(1 - CL_b)$ and CL_{s+b} quantify the consistency of the data with the "background-only" and the "signal+background" hypotheses, respectively, whereas CL_s is the confidence level used to exclude the signal hypothesis. An observation of CL_s value smaller than 5% means that the signal hypothesis is excluded at 95% confidence level. The analysis performance is quantified with the expected median confidence level CL_{med} [25].

The main sources of systematic uncertainties are the detector resolution, the selection procedure, theoretical uncertainties and Monte Carlo statistics. The overall systematic uncertainty is estimated to be 3% on the prediction for the expected signal and 7% on the background.

The analyses presented in this paper are combined with the $hZ \to b\bar{b}\nu\bar{\nu}$ and $hZ \to b\bar{b}\ell^+\ell^-$ ($\ell = e, \mu$) analyses used in the Standard Model Higgs searches [23]. The results of previous searches [4] at lower $\sqrt{s}$ are also included.

Generally, good agreement between the observation and the background expectation is found in the L3 combined data. There are several regions in the (m_A,m_h) plane where excesses of more than 2σ are observed in the data, however in each case the effect arises from candidates of a single topology. The largest excess, amounting to 2.4σ, is found at (m_A,m_h) $\sim$ (68,68) GeV. This effect is mainly caused by candidates of the $hA \to b\bar{b}b\bar{b}$ topology collected at $\sqrt{s} = 189$ GeV in the year 1998. There are also excesses with the significance of about 2σ observed at (m_A,m_h) $\sim$ (82,75) GeV and $m_h \sim 99$ GeV. The excess at (m_A,m_h) $\sim$ (82,75) GeV results mainly from the $hZ \to b\bar{b}q\bar{q}$ candidates found in the data samples of the years 1998 and 2000. The excess at $m_h \sim 99$ GeV arises due to several candidates in the $hZ \to b\bar{b}\ell^+\ell^-(\ell = e, \mu)$ channels found at $\sqrt{s}$ between 192 GeV and 202 GeV in the data of the year 1999. Furthermore, all these excesses, except the region of $m_h \sim 99$ GeV, are below the expectation for a signal from the neutral Higgs bosons of the MSSM. Regarding them as statistical fluctuations, the data are interpreted in terms of exclusion of the MSSM parameter regions.

5.1 Limits in the "m_h-max" and "No mixing" Scenarios

Figure 4 shows the area of the (tanβ,m_h) and (tanβ,m_A) planes excluded at 95% confidence level for the "m_h-max" and "no mixing" scenarios. In the "m_h-max" scenario lower limits on

the masses of h and A bosons are set at 95% confidence level,

$$m_{\mathrm{A}} > 86.5 \text{ GeV}, \qquad m_{\mathrm{h}} > 86.0 \text{ GeV},$$

for every tanβ value considered. The expected values in the absence of a signal are $m_{\mathrm{A}} >$ 88.6 GeV and $m_{\mathrm{h}} > 88.4$ GeV. For $0.55 < \tan\beta < 2.2$ the A boson is excluded up to a mass of 1 TeV thus allowing to rule out this tanβ range.

In the "no mixing" scenario the combined results establish lower mass bounds at 95% of:

$$m_{\mathrm{A}} > 86.3 \text{ GeV}, \qquad m_{\mathrm{h}} > 85.5 \text{ GeV}.$$

The expected limits are $m_{\mathrm{A}} > 88.6$ GeV and $m_{\mathrm{h}} > 88.5$ GeV. Here the tanβ range between 0.4 and 5.4 is excluded at 95% confidence level. A downward fluctuation of about 1σ compared to the background expectation is observed in the data at (m_{A},m_{h}) $\sim$ (90,90) GeV. There is a deficit of candidates in the $\mathrm{hA} \to \mathrm{b\bar{b}b\bar{b}}$ channel at $\sqrt{\mathrm{s}} = 203$ - 209 GeV resulting in an observation of the $\mathrm{CL_s}$ value smaller than 5% although no exclusion of this region at 95% confidence level is expected. This effect explains the irregularity in the exclusion plots at high tanβ and m_{h} between 86 GeV and 91 GeV. The excess in the $\mathrm{hZ} \to \mathrm{b\bar{b}}\ell^+\ell^-$ channel discussed above and in the $\mathrm{hZ} \to \mathrm{b\bar{b}q\bar{q}}$ channel in the data of the year 1999 result in a sizable reduction of the experimentally excluded range of tanβ for the mass range 90 GeV $\lesssim m_{\mathrm{h}} \lesssim$ 100 GeV in both scenarios discussed. The area at $\tan\beta < 0.8$ and $m_{\mathrm{A}} < 40$ GeV which was not previously excluded in the "no mixing" scenario [4] is now excluded using the results of the $\mathrm{hZ} \to \mathrm{AAq\bar{q}}$ search[2)].

5.2 Limits in the "Large-μ" Scenario

In the "large-μ" scenario there are regions of the (tanβ,m_{A}) plane where the hA process is inaccessible and the hZ process is suppressed by a small value of $\sin^2(\beta - \alpha)$. However, the heavy CP even Higgs boson H is expected to be produced there via the Higgs-strahlung process. Hence, the loss of the sensitivity for the h boson can be compensated by reinterpreting the hZ analyses in the context of the HZ search. This is illustrated in Figures 5a and 5b which present $(1 - \mathrm{CL_{med}})$ and $(1 - \mathrm{CL_s})$ confidence levels calculated as a function of m_{A} at tanβ =15 in the context of the searches for the h and H bosons. Searches for the h boson alone lack sensitivity in the m_{A} range 90 GeV $\lesssim m_{\mathrm{A}} \lesssim$ 108 GeV. But inclusion of the HZ search results extends the region of sensitivity leaving only the range 90 GeV $\lesssim m_{\mathrm{A}} \lesssim$ 98 GeV unexcluded. However, since all the analyses, except for the $\mathrm{hZ} \to \tau^+\tau^-\mathrm{q\bar{q}}$ channel, are optimised for the Higgs boson decays to $\mathrm{b\bar{b}}$, they do not provide sufficient sensitivity to the parameter regions where effective couplings $\mathrm{Hb\bar{b}}$ and $\mathrm{hb\bar{b}}$ are suppressed. For tanβ equal 15 and m_{A} around 94 GeV, this situation can be seen in Figures 5a and 5b.

Exclusion plots in the (tanβ,m_{h}) and (tanβ,m_{A}) planes for the "large-μ" scan are presented in Figures 5c and 5d, respectively. The limits on Higgs boson masses are

$$m_{\mathrm{h}} > 84.5 \text{ GeV}, \qquad m_{\mathrm{A}} > 86.5 \text{ GeV}.$$

The expected values are 87.2 GeV and 89.2 GeV, respectively. Furthermore, the range $0.7 < \tan\beta < 6.7$ is excluded. The experimentally allowed area spreading from $\tan\beta = 15$ to $\tan\beta = 50$

[2)] The $\mathrm{hZ} \to \mathrm{AAq\bar{q}}$ analysis was used instead of the four-jet one whenever it provided better sensitivity, i.e. gave smaller values of $\mathrm{CL_{med}}$.

and inclined with respect to the m_{A} axis corresponds to reduced $\mathrm{Hb\bar{b}}$ or $\mathrm{hb\bar{b}}$ couplings. The unexcluded region at $m_{\mathrm{A}} \sim 88$ GeV and $\tan\beta \sim 15$ is caused by slight upward fluctuation in the data coming mainly from the $\mathrm{hA} \to \mathrm{b\bar{b}b\bar{b}}$ candidates selected from data collected during the year 2000. The experimentally allowed vertical narrow band at $m_{\mathrm{A}} = 107$ - 110 GeV and $\tan\beta \gtrsim 10$ represents the region where the hA production is kinematically inaccessible and $\cos^2(\beta-\alpha) \approx \sin^2(\beta-\alpha) \approx 0.5$ so that both the hZ and HZ production cross sections are reduced by a factor of 2 with respect to the HZ production cross section in the SM. Although the L3 combined search has a sensitivity for exclusion of this critical region as can be seen from Figure 5a, the expected median confidence level is only slightly lower than 5% and an insignificant upward fluctuation observed in the data pushes the observed confidence level, $\mathrm{CL_s}$, above 5%, thus not allowing to exclude this region at 95% confidence level. Finally, the allowed area at $\tan\beta$ between 6.7 and 10 and m_{h} between 90 and 100 GeV arises due to the excesses already pointed out above.

6 Summary

In the search for the neutral Higgs bosons, performed in three MSSM benchmark scenarios at center-of-mass energies up to 209 GeV, no signal is found. The lower mass limits, obtained for $\tan\beta$ greater than 0.7 in all scenarios, are $m_{\mathrm{A}} > 86.3$ GeV and $m_{\mathrm{h}} > 84.5$ GeV at 95% confidence level.

References

[1] H. P. Nilles, Phys. Rep. **110** (1984) 1;
H. E. Haber and G. L. Kane, Phys. Rep. **117** (1985) 75;
R. Barbieri, Riv. Nuovo Cim. **11 n°4** (1988) 1.

[2] J.F. Gunion *et al.*, in The Higgs Hunter's Guide, (Addison Wesley, 1990), p. 191.

[3] D.E. Groom *et al.*, Eur. Phys. J. **C 15** (2000) 1.

[4] L3 Collaboration, M. Acciarri *et al.*, Phys. Lett. **B 503** (2001) 21.

[5] OPAL Collaboration, G. Abbiendi *et al.*, Eur. Phys. J. **C 12** (2000) 567;
ALEPH Collaboration, A. Heister *et al.*, Phys. Lett. **B 526** (2002) 191;
DELPHI Collaboration, J. Abdallah *et al.*, Eur. Phys. J. **C 23** (2002) 409.

[6] L3 Collab., B. Adeva *et al.*, Nucl. Instr. Meth. **A 289** (1990) 35;
J.A. Bakken *et al.*, Nucl. Instr. Meth. **A 275** (1989) 81;
O. Adriani *et al.*, Nucl. Instr. Meth. **A 302** (1991) 53;
B. Adeva *et al.*, Nucl. Instr. Meth. **A 323** (1992) 109;
K. Deiters *et al.*, Nucl. Instr. Meth. **A 323** (1992) 162;
M. Chemarin *et al.*, Nucl. Instr. Meth. **A 349** (1994) 345;
M. Acciarri *et al.*, Nucl. Instr. Meth. **A 351** (1994) 300;
G. Basti *et al.*, Nucl. Instr. Meth. **A 374** (1996) 293;
A. Adam *et al.*, Nucl. Instr. Meth. **A 383** (1996) 342.

[7] M. Carena, S. Heinemeyer, C.E.M. Wagner, G. Weiglein, CERN-TH/99-374.

[8] S.Heinememeyer, W.Hollik, G. Weiglein, Eur. Phys. J. **C9** (1999) 343.

[9] S. Heinemeyer, W. Hollik, G. Weiglein, Phys. Rev. **D 58** (1998) 091701;
S. Heinemeyer, W. Hollik, G. Weiglein, Phys. Lett. **B 440** (1998) 296.

[10] W. Loinaz and J.D. Wells, Phys. Lett. **B 445** (1998) 178;
H. Baer and J.D. Wells, Phys. Rev. **D 57** (1998) 4446.

[11] M. Carena, S. Mrenna, C.E.M. Wagner, Phys. Rev. **D 60** (1999) 075010.

[12] M. Carena, M. Quiros and C. E. M. Wagner, Nucl. Phys. **B 461** (1996) 407.

[13] M. Carena *et al.*, Nucl. Phys. **B 580** (2000) 29.

[14] P. Janot, "The HZHA generator", in "Physics at LEP2", CERN Report 96-01 (1996), Version 3, released in December 1999,
`http://alephwww.cern.ch/~janot/Generators.html`.

[15] PYTHIA versions 5.722 and 6.1 are used.
T. Sjöstrand, Preprint CERN-TH/7112/93 (1993), revised August 1995; Comp. Phys. Comm. **82** (1994) 74; Preprint hep-ph/0001032 (2000).

[16] KK2f version 4.13 is used;
S. Jadach, B.F.L. Ward and Z. Wąs, Comp. Phys. Comm. **130** (2000) 260.

[17] KORALW version 1.33 is used.
S. Jadach *et al.*, Comp. Phys. Comm. **94** (1996) 216;
S. Jadach *et al.*, Phys. Lett. **B 372** (1996) 289.

[18] KORALZ version 4.02 is used.
S. Jadach, B.F.L. Ward and Z. Wąs, Comp. Phys. Comm. **79** (1994) 503.

[19] PHOJET version 1.05 is used.
R. Engel, Z. Phys. **C 66** (1995) 203;
R. Engel and J. Ranft, Phys. Rev. **D 54** (1996) 4244.

[20] F. A. Berends, R. Pittau and R. Kleiss, Comp. Phys. Comm. **85** (1995) 437.

[21] GEANT version 3.15 is used;
R. Brun *et al.*, Preprint CERN DD/EE/84-1 (1984), revised 1987.

[22] H. Fesefeldt, Report RWTH Aachen PITHA 85/02 (1985).

[23] L3 Collaboration, P. Achard *et al.*, Phys. Lett. **B 517** (2001) 319.

[24] S. Bethke *et al.*, Nucl. Phys. **B 370** (1992) 310.

[25] A. Read, "Modified Frequentist Analysis of Search Results" in *Workshop on Confidence Limits*, eds. F. James, L.Lyons and Y.Perrin, CERN 2000-05, p. 81. The expected median confidence level CL_{med} is defined as CL_s obtained by replacing the observed value of the log-likelihood ratio -2lnQ by its background median value.

[26] OPAL Collaboration, G. Alexander *et al.*, Z. Phys. **C 73** (1997) 189.

Scenario	M_{SUSY} (GeV)	M_2 (GeV)	μ (GeV)	X_t (GeV)	M_3 (GeV)
"m_h-max"	1000	200	-200	$2M_{SUSY}$	800
"no mixing"	1000	200	-200	0	800
"large-μ"	400	400	1000	-300	200

Table 1: Values of the MSSM parameters for the three representative scenarios considered in this paper.

"m_h-max" scenario		
(m_A,m_h) (GeV)	(90,90)	(165,110)
tanβ	25	3
Preselection		
Background	2044.5	
Data	2096	
$\epsilon(hA \to b\bar{b}b\bar{b})$	94%	-
$\epsilon(hZ \to b\bar{b}q\bar{q})$	89%	92%
hA signal	7.17	-
hZ signal	0.66	18.4
Selection		
Analysis branch	hA hZ	hZ
Background	28.9 258.7	120.1
Data	25 275	121
$\epsilon(hA \to b\bar{b}b\bar{b})$	56% 19%	-
$\epsilon(hZ \to b\bar{b}q\bar{q})$	25% 37%	63%
hA signal	4.26 1.45	-
hZ signal	0.18 0.28	12.6
s/b > 0.05		
Background	21.3	42.1
Data	18	42
$\epsilon(hA \to b\bar{b}b\bar{b})$	56%	-
$\epsilon(hZ \to b\bar{b}q\bar{q})$	28%	55%
hA signal	4.29	-
hZ signal	0.21	11.0

Table 2: The number of data, expected background, expected signal events and signal efficiencies in the four-jet channel after preselection, after final selection and after applying a cut on the final discriminants corresponding to a signal-to-background ratio greater than 0.05. This cut is used to calculate the confidence levels. Numbers are given for two Higgs mass hypotheses in the "m_h-max" scenario and correspond to the entire sample of the year 2000.

"m_{h}-max" scenario		
(m_{A},m_{h}) (GeV)	(90,90)	(165,110)
tanβ	25	3
Selection		
Background	27.4	6.39
Data	28	8
$\epsilon(\mathrm{hA} \to \mathrm{b\bar{b}}\tau^+\tau^-)$	41%	-
$\epsilon(\mathrm{hA} \to \tau^+\tau^-\mathrm{b\bar{b}})$	41%	-
$\epsilon(\mathrm{hZ} \to \mathrm{b\bar{b}}\tau^+\tau^-)$	22%	33%
$\epsilon(\mathrm{hZ} \to \tau^+\tau^-\mathrm{q\bar{q}})$	21%	32%
hA signal	0.50	-
hZ signal	0.03	0.78
s/b > 0.05		
Background	1.55	2.75
Data	2	3
$\epsilon(\mathrm{hA} \to \mathrm{b\bar{b}}\tau^+\tau^-)$	34%	-
$\epsilon(\mathrm{hA} \to \tau^+\tau^-\mathrm{b\bar{b}})$	30%	-
$\epsilon(\mathrm{hZ} \to \mathrm{b\bar{b}}\tau^+\tau^-)$	19%	30%
$\epsilon(\mathrm{hZ} \to \tau^+\tau^-\mathrm{q\bar{q}})$	14%	29%
hA signal	0.39	-
hZ signal	0.02	0.70

Table 3: The number of data, expected background, expected signal events and signal efficiencies in the channels containing tau leptons after selection and after applying a cut on the final discriminants corresponding to a signal-to-background ratio greater than 0.05. This cut is used to calculate the confidence levels. Numbers are given for two Higgs mass hypotheses in the "m_{h}-max" scenario and correspond to the entire sample of the year 2000.

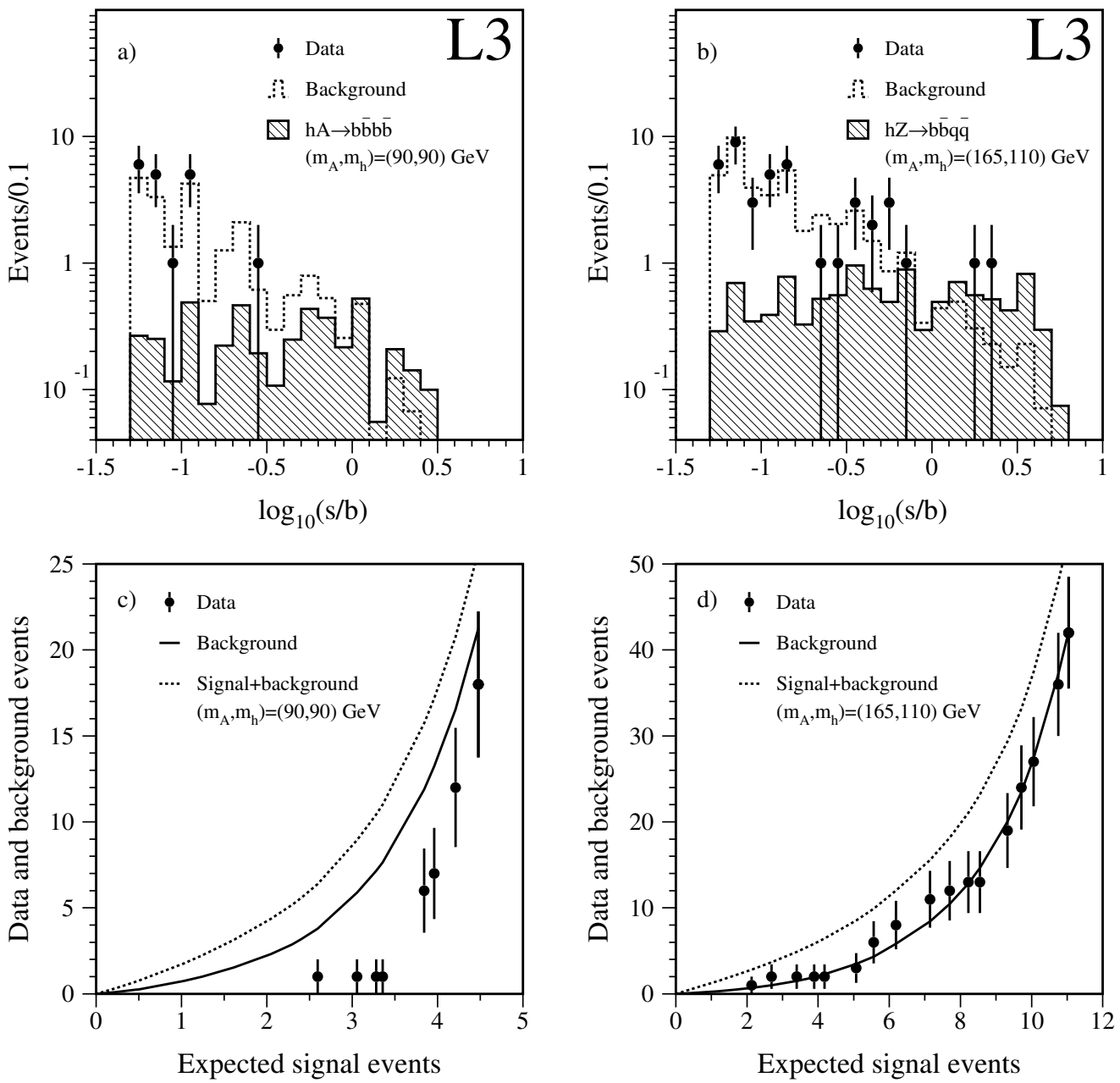

Figure 1: The distribution of data, expected background and expected signal events as a function of the logarithm of a signal-to-background ratio, $\log_{10}(\mathrm{s/b})$ in the four-jet channel for the Higgs boson mass hypotheses a) $(m_{\mathrm{A}},m_{\mathrm{h}}) = (90,90)$ GeV and b) $(m_{\mathrm{A}},m_{\mathrm{h}}) = (165,110)$ GeV. The points are data at $\sqrt{s} > 203$ GeV, the dashed lines are the expected background and the hatched histograms are the expected signal. Data and expected background events as a function of the expected signal are shown in figures c) and d) for the $(m_{\mathrm{A}},m_{\mathrm{h}}) = (90,90)$ GeV and $(m_{\mathrm{A}},m_{\mathrm{h}}) = (165,110)$ GeV hypotheses, respectively. These curves are obtained by integrating the $\log_{10}(\mathrm{s/b})$ distributions from the right to the left side.

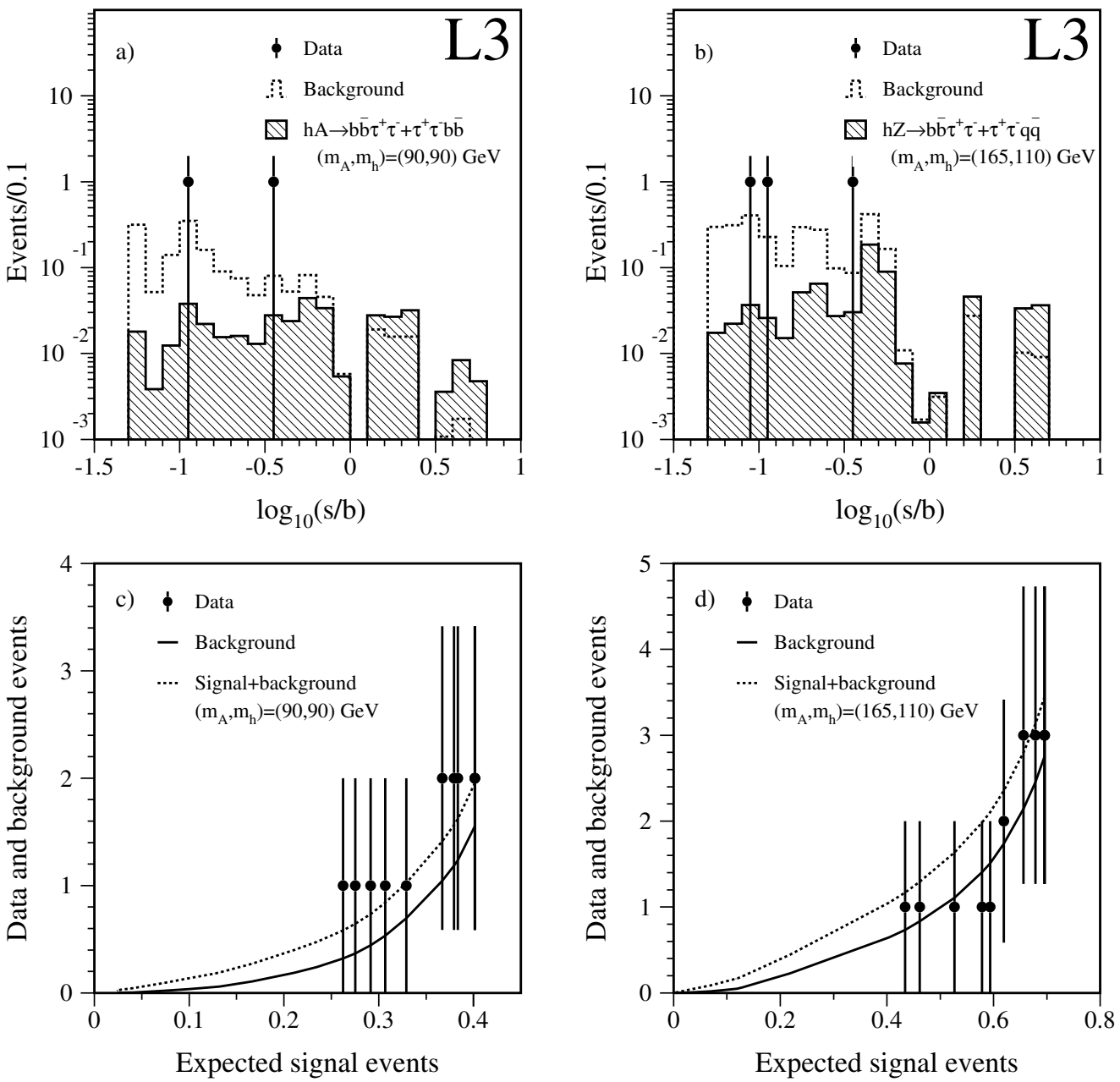

Figure 2: The distribution of data, expected background and expected signal events as a function of the logarithm of a signal-to-background ratio, $\log_{10}$(s/b), in the channels containing tau leptons for the Higgs boson mass hypotheses a) ($m_{\rm A}$,$m_{\rm h}$) = (90,90) GeV and b) ($m_{\rm A}$,$m_{\rm h}$) = (165,110) GeV. The points are data at $\sqrt{\rm s} > 203$ GeV, the dashed lines are the expected background and the hatched histograms are the expected signal. Data and expected background events as a function of the expected signal are shown in figures c) and d) for the ($m_{\rm A}$,$m_{\rm h}$) = (90,90) GeV and ($m_{\rm A}$,$m_{\rm h}$) = (165,110) GeV hypotheses, respectively. These curves are obtained by integrating the $\log_{10}$(s/b) distributions from the right to the left side.

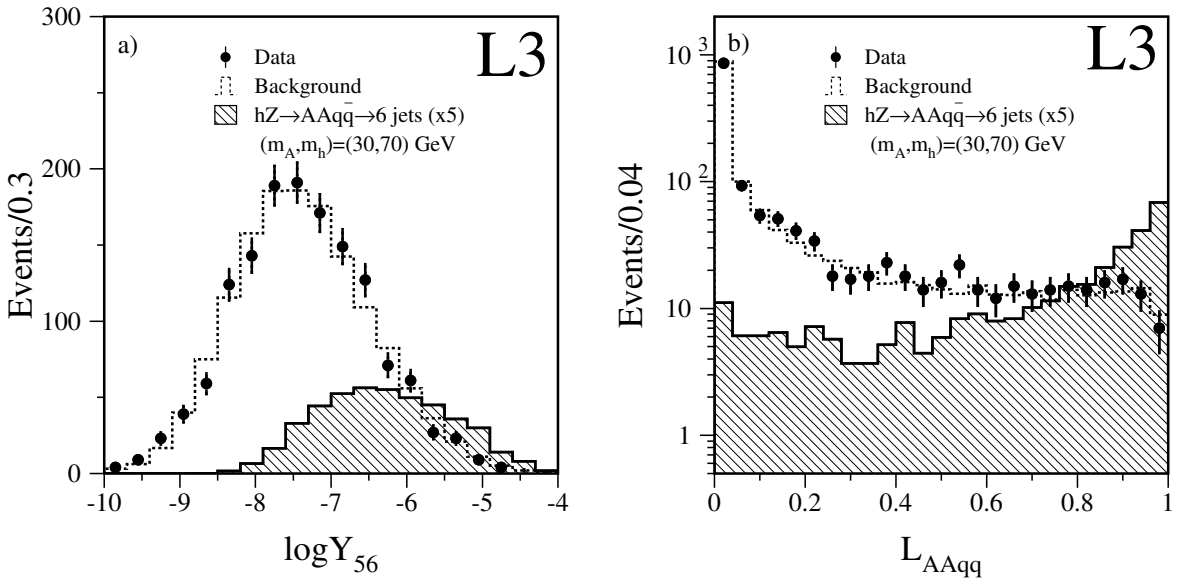

Figure 3: Distributions of a) $\log Y_{56}$ and b) L_{AAqq} in the $hZ \to AAq\bar{q} \to q\bar{q}q'\bar{q}'q''\bar{q}''$ channel. The points are data collected in the year 2000, the dashed lines are the expected background and the hatched histograms are the signal corresponding to the Higgs boson mass hypothesis (m_A,m_h) = (30,70) GeV. The signal expectation is calculated within the "no mixing" scenario at $\tan\beta = 0.75$ and multiplied by a factor of 5.

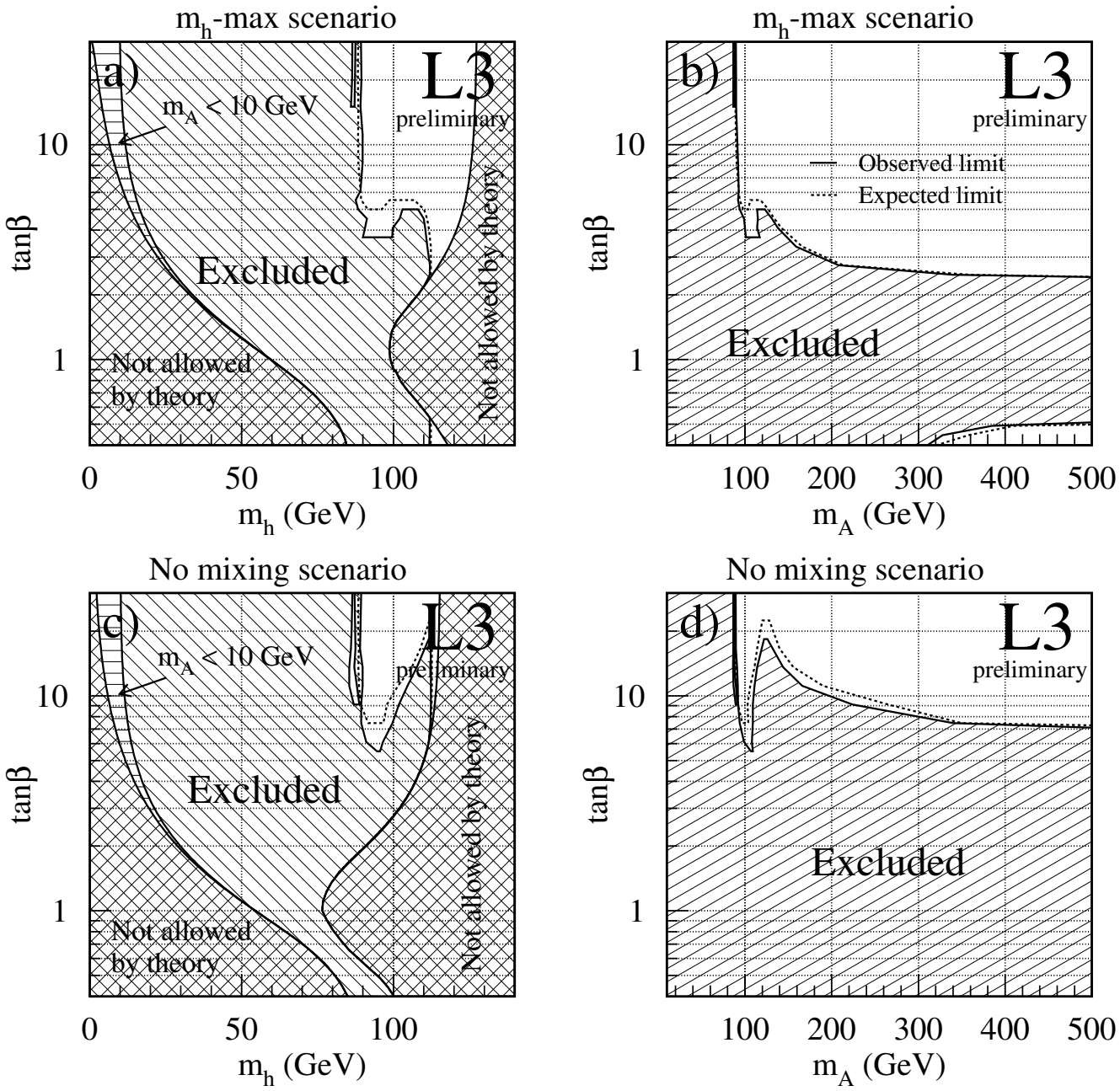

Figure 4: Exclusion plots in the (tanβ,$m_{\rm h}$) and (tanβ,$m_{\rm A}$) planes at 95% confidence level for the "$m_{\rm h}$-max" and "no mixing" scenarios. The hatched area represents the exclusion and the crossed area is not allowed by theory. The horizontally hatched area corresponds to $m_{\rm A}<$ 10 GeV and was previously excluded by LEP [26]. The dashed line indicates the expected exclusion in the absence of a signal.

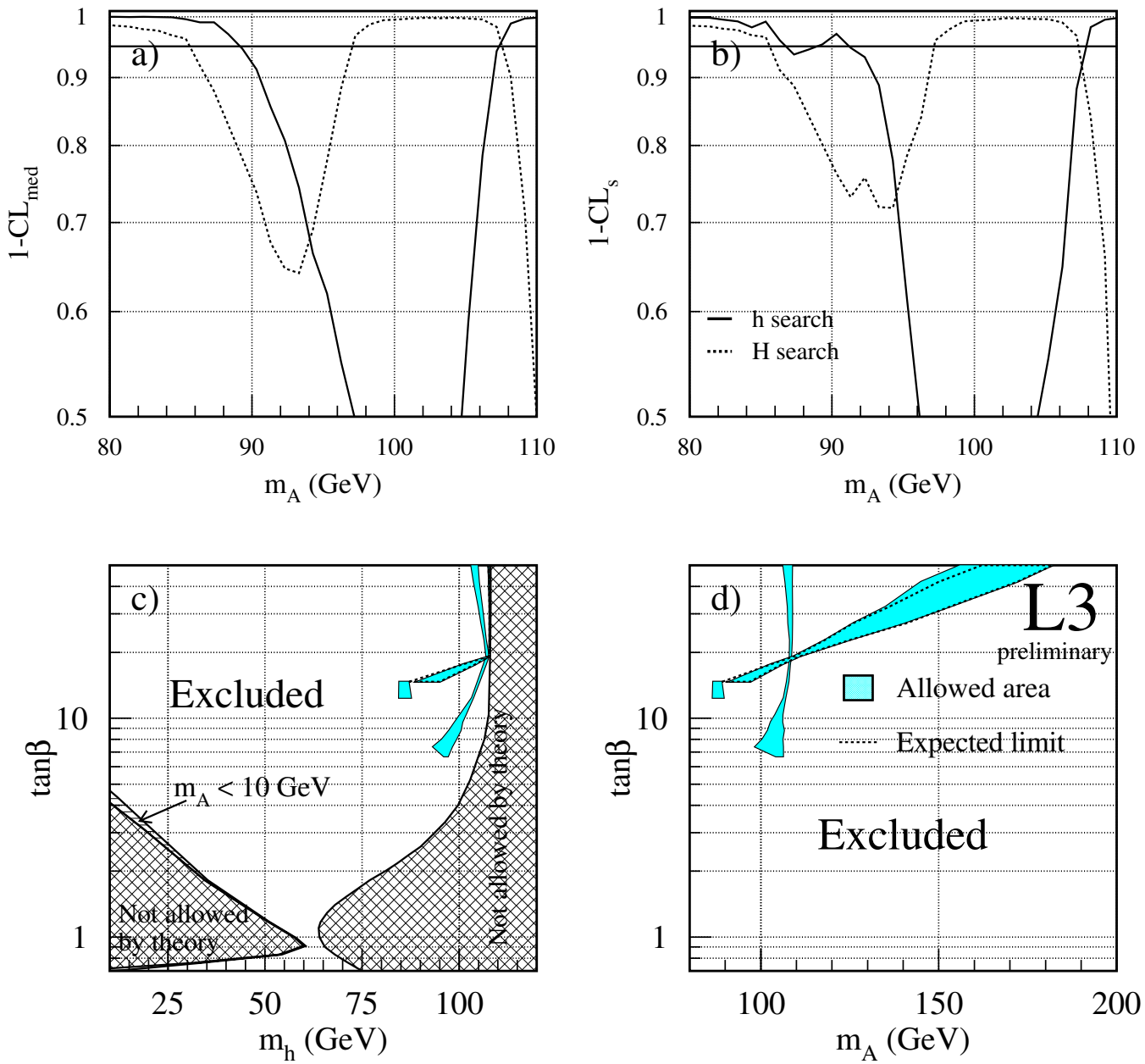

Figure 5: Confidence levels and exclusion regions in the "large-μ" scenario. Confidence levels a) $(1 - \mathrm{CL_{med}})$ and b) $(1 - \mathrm{CL_s})$ as a function of m_A at $\tan\beta = 15$ obtained for the h boson (solid line), and the H boson (dashed line) searches. Excluded regions in the c) ($\tan\beta$,m_h) and d) ($\tan\beta$,m_A) planes. The hatched area is theoretically inaccessible. The open area is excluded at 95% confidence level. The shaded area is experimentally allowed. The dashed line represent the expected boundary of the unexcluded region in the absence of the signal.